SCIENTIFIC REP🅞RTS

OPEN

Preparation and characterization of Sn/La co-doped TiO$_2$ nanomaterials and their phase transformation and photocatalytic activity

Xiaodong Zhu [ID][1,3,4], Lingxiu Pei[1], Ranran Zhu[1], Yu Jiao[2,3], Renyong Tang[5] & Wei Feng[1,4]

The pure, tin (Sn)-doped, lanthanum (La)-doped and Sn/La co-doped titanium dioxide (TiO$_2$) nanomaterials were synthesized using sol-gel method followed by calcination at the temperature of 360 °C, 450 °C and 600 °C, respectively. The structures of the nanomaterials were characterized by X-ray diffraction (XRD), Thermogravimetric (TG), Differential Thermal Analysis (DTA), Scanning Electron Microscopy (SEM), Energy Dispersive Spectrum (EDS), Transmission Electron Microscopy (TEM), X-ray Photoelectron Spectrum (XPS), Diffuse Reflectance Spectrum (DRS), Photoluminescence Spectrum (PL), Brunauer-Emmett-Teller Measurements (BET), respectively. The photocatalytic property of the photocatalysts under UV light was evaluated through the degradation of Rhodamine B (RhB). The results show that the anatase-rutile phase transition is promoted by Sn-doping while La-doping retards the phase transition. However, La doping plays a major role in the process of phase transformation. The photocatalytic activity of pure TiO$_2$ is affected by annealing temperature remarkably and the optimal annealing temperature is 450 °C. The photocatalytic activity of TiO$_2$ is enhanced significantly by Sn and La doping at three different temperatures. Sn/La-TiO$_2$ exhibits the highest degradation rates and the fastest reaction rates probably owing to the synergistic effect of Sn^{4+} and La^{3+} ions in inhibiting the recombination of photogenerated electron-hole pairs. The formation of extra surface hydroxyl groups and additional surface area are also beneficial for the photocatalytic activity.

Environmental pollution is an increasingly serious problem, which restricts the development of economy severely. Photocatalytic technology is an effective way to solve the problem and several semiconductor photocatalysts have been used for decomposing organic pollutants such as zinc oxide[1], cadmium sulfide[2], carbon nanoparticle[3], tungsten trioxide[4] and so on. Among numerous candidate compounds, TiO$_2$ has been widely used owing to its high photocatalytic activity, non-toxicity, low cost and stable chemical property[5–8]. However, pure TiO$_2$ has two main faults such as low utilization of solar energy because of the wide band gap and low quantum yields since photogenerated electron-hole pairs recombine fast[9,10]. In order to improve the photocatalytic activity of pure TiO$_2$, researchers adopt some strategies such as depositing with noble metals[11–13], combining with other semiconductors[14–17] and doping metal[18–20] or nonmetal elements[21,22].

Doping with La element boosts the photocatalytic activity of TiO$_2$ efficiently because La ions are able to capture photogenerated electrons, prolong the lifetime of photogenerated electron-hole pairs and increase the thermostability of anatase phase which has higher photocatalytic activity than that of rutile phase[23,24]. Xin et al.[25] reported that the discoloration rate of RhB was enhanced by La doping of the TiO$_2$ photoelectrode. TiO$_2$ doping with Sn is also an effective method to enhance photocatalytic activity since the coupling of TiO$_2$ with SnO$_2$ decreases the recombination of photogenerated electron-hole pairs and thus improves charge separation[20,26,27]. Bhange et al.[28] have synthesized a series of Sn-doped TiO$_2$ particles with different concentrations and photocatalytic tests show all the Sn-doped TiO$_2$ have higher photocatalytic activity than that of pure TiO$_2$. It is reasonable to

[1]College of Mechanical Engineering, Chengdu University, Chengdu, 610106, China. [2]College of Science, Xichang University, Xichang, 615013, China. [3]College of Materials and Chemistry & Chemical Engineering, Chengdu University of Technology, Chengdu, 610059, China. [4]Sichuan Engineering Research Center for Powder Metallurgy, Chengdu University, Chengdu, 610106, China. [5]College of Pharmacy and Biological Engineering, Chengdu University, Chengdu, 610106, China. Correspondence and requests for materials should be addressed to X.Z. (email: xiaodangjia21@126.com) or W.F. (email: fengwei1981_829@foxmail.com)

suppose that doping with two dopants will lead to a synergistic effect and increase photocatalytic activity owing to their respective advantages. There are several reports about co-doped TiO$_2$ which have proved that doping with two dopants shows higher photocatalytic activity than the single one[23,29-34].

In the study of co-doped TiO$_2$, most researchers focus on the concentration of dopants, however, research on the influence of heat treatment temperature is relatively few. It is generally known that heat treatment has a significant impact on the photocatalytic activity of TiO$_2$ because crystalline phase and grain size of TiO$_2$ are affected greatly by annealing temperature. Meanwhile, ion doping will impact phase structure and grain size evidently. The reports have mentioned that anatase-rutile phase transition will be restrained by La doping[25] while it is promoted by Sn doping[26,28]. However, the phase transformation is not quite clear when Sn and La are doped together. Therefore, the purposes of this work was to synthesize Sn/La co-doped TiO$_2$ nanomaterials and investigate their anatase-rutile phase transition as well as photocatalytic activities under UV light at different temperatures. For comparison, Sn-doped, La-doped and pure TiO$_2$ nanomaterials were also prepared and investigated. For simplicity, Sn-doped, La-doped, and Sn/La co-doped TiO$_2$ are labeled as Sn-TiO$_2$, La-TiO$_2$ and Sn/La-TiO$_2$, respectively.

Experiment

Preparation of pure and doped TiO$_2$ nanomaterials.
All the TiO$_2$ nanomaterials were synthesized via a sol-gel route. In a typical synthesis of pure TiO$_2$, solution A and B were prepared firstly. Solution A consisted of 15 mL tetrabutyl titanate and 30 mL absolute ethanol. Solution B was made from 5 mL deionized water, 7.5 mL acetic acid and 15 mL absolute ethanol. Solution B was added dropwise to solution A with vigorous stirring. The resulting sol was undergone aging for several hours to form gel. Afterwards, the gel was dried at 80 °C for 12 h and the resulting powders were annealed for 2 h at the temperature of 360 °C, 450 °C and 600 °C, respectively. The Sn-TiO$_2$ and La-TiO$_2$ were synthesized by the same procedure with certain amounts of SnCl$_4$.5H$_2$O or La(NO$_3$)$_3$.6H$_2$O being added into solution B to obtain required doping concentration. The Sn/Ti molar ratios of Sn-TiO$_2$ were 1%, 3%, 6%, 9% and the La/Ti molar ratios of La-TiO$_2$ were 0.2%, 0.5%, 1%, 2%. Sn/La-TiO$_2$ was prepared by the same way and the Sn/Ti, La/Ti molar ratios were 3% and 0.5%, respectively.

Characterization.
The crystal structures of the nanomaterials were analyzed using an X-ray diffractometer (XRD, DX-2700, China). Thermogravimetric and differential thermal analysis (TG-DTA) were performed using a thermal analyzer (STA409PC, Germany). Surface morphologies and element compositions were characterized by a field-emission scanning electron microscopy (FEI-Inspect F50, USA) equipped with an energy dispersive X-ray spectrometer (EDS). TEM and HRTEM images were obtained using a Tecnai G2 F20 transmission electron microscope with an acceleration voltage of 200 kV. X-ray photoelectron spectra (XPS) were recorded on a spectrometer (XSAM800, Britain) to examine the chemical states. UV-Vis diffuse reflectance spectra (DRS) were collected on a spectrophotometer (UV-3600, Japan). Photoluminescence (PL) spectra were measured by a luminescence spectrometer (F-4600, Japan) with a 150 W Xenon lamp as an excitation source. Surface areas were tested by using the Brunauer-Emmett-Teller (BET) theory to the nitrogen adsorption-desorption data.

Photocatalytic activity measurement.
The photocatalytic activity of the prepared nanomaterials under UV light was evaluated from the degradation of Rhodamine B (RhB). 300 mL 10 mg/L RhB solution was taken into a beaker as an objective degradation pollutant and 0.3 g TiO$_2$ was added as photocatalysts. The mixed liquid was stirring for 30 min in dark to establish an adsorption-desorption equilibrium before illumination. It was then photo-irradiated by using a 250 W high-pressure mercury lamp (main emission wavelength 365 nm, light intensity 35 mW/cm^2) as UV light source. The distance between lamp source and beaker was fixed at 10 cm. The change in the concentration of RhB was tested every 30 min by measuring absorbance at the maximum absorptive wavelength (553 nm) using a UV-Vis spectrophotometer (UV6100A, China) and the whole test lasted 180 min. The degradation rate (D) of RhB was calculated by equation: D = (A$_0$ − A$_t$)/A$_0$, where A$_0$ and A$_t$ are the initial absorbance (at 553 nm) and absorbance at time "t".

Results and Discussion

XRD analysis.
Figure 1 shows the XRD patterns of TiO$_2$ nanomaterials at different temperature. All samples show peaks corresponding to anatase phase at the temperature of 360 °C and 450 °C. Compared to 360 °C, the intensity of peaks at 450 °C increases and the width of peaks becomes narrow, which imply that crystalline integrity improves with increase in temperature[19,35]. Pure TiO$_2$ forms rutile phase when the heat treatment temperature is up to 600 °C. It is clear that the peak intensity of rutile phase of Sn-TiO$_2$ is stronger than that of pure TiO$_2$. However, there is no peak of rutile phase observed in La-TiO$_2$, which indicates that anatase-rutile phase transition is promoted by Sn doping while it is suppressed by La doping. This is in agreement with the literature[25,26,28]. Ding et al.[36] believe that the melting point of doped element oxides will affect anatase-rutile phase transition. The melting point of SnO$_2$ is 1127 °C, which is lower than that of TiO$_2$ (1640 °C), thus Sn as doping element promotes the transition. Meanwhile, the melting point of La$_2$O$_3$ is 2217 °C, which is higher than 1640 °C, as a result, La doping can retard the transition. As depicted in Fig. 1(c), a weak peak which corresponds to rutile (110) plane appears in the pattern of Sn/La-TiO$_2$, indicates that the amount of rutile is less compared to pure TiO$_2$. Obviously, the retarding effect by La doping plays a major role in the process of anatase-rutile phase transition although the dopant concentration of La (0.5%) is less than Sn (3%). The anatase/rutile weight ratios were calculated by the following equation[37]:

$$X_R = (1 + 0.8(I_A/I_R))^{-1}$$

where X$_R$ is the weight fraction of rutile, I$_A$ and I$_R$ are the relative strength of anatase (101) plane and rutile (110) plane, respectively. The average grain size (D) was calculated by Scherer's formula[38]:

Temperature	Samples	Crystal phase	Grain size/nm
360 °C	pure TiO$_2$	Anatase	13.2
	Sn-TiO$_2$	Anatase	11.5
	La-TiO$_2$	Anatase	12.9
	Sn/La-TiO$_2$	Anatase	11
450 °C	pure TiO$_2$	Anatase	14.9
	Sn-TiO$_2$	Anatase	13.2
	La- TiO$_2$	Anatase	13.3
	Sn/La-TiO$_2$	Anatase	11.3
600 °C	pure TiO$_2$	Anatase (67.0%)/Rutile (33.0%)	29.3/51.2
	Sn-TiO$_2$	Anatase (30.9%)/Rutile (69.1%)	15.9/39.8
	La-TiO$_2$	Anatase	15.5
	Sn/La-TiO$_2$	Anatase (95.8%)/Rutile (4.2%)	13.6/62.1

Table 1. Crystal phase and grain size of TiO$_2$ nanomaterials.
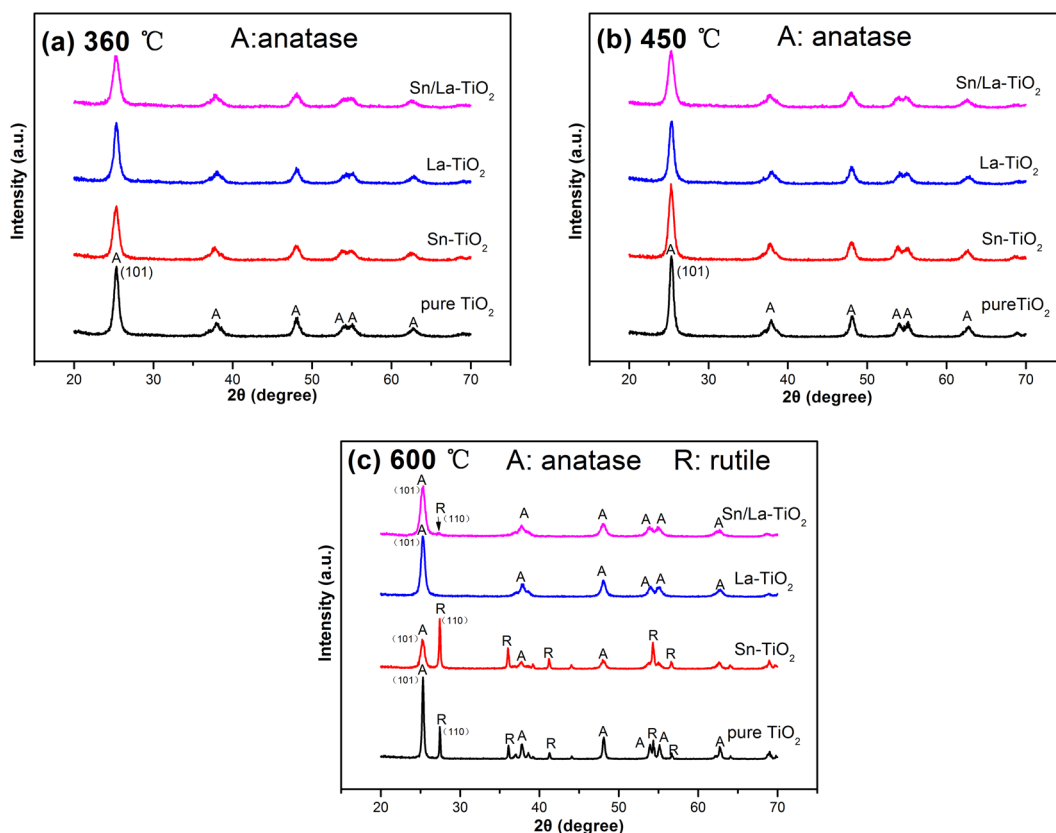
Figure 1. XRD patterns of pure TiO$_2$, Sn-TiO$_2$, La-TiO$_2$ and Sn/La-TiO$_2$ annealed at 360 °C (**a**), 450 °C (**b**) and 600 °C (**c**).

$$D = 0.89\lambda/\beta \cos\theta$$

where λ is the wavelength of Cu Kα used, β is the full with at half maximum of the XRD peak and θ is the Bragg diffraction angle. The results are shown in Table 1. It clearly shows that the grain size of TiO$_2$ decreases by doping and Sn/La-TiO$_2$ presents the smallest grain size at the same temperature.

TG-DTA analysis.   Thermal analyses of pure TiO$_2$ (a), Sn-TiO$_2$ (b), La-TiO$_2$ (c) and Sn/La-TiO$_2$ (d) are depicted in Fig. 2. Left side of Y-axis represents the weight loss of samples. Right side of Y-axis represents exothermic and endothermic of samples during the heating process. The weight loss of all samples consists of three steps. In detail, the loss in the first step mainly derives from the evaporation of physically adsorbed water[26]. The combustion of organic compounds can be responsible for the second weight loss step. The third step of weight loss can be attributed to the dehydroxylation of the gel[31]. The exothermic peak at 578 °C in the DTA curve of pure TiO$_2$
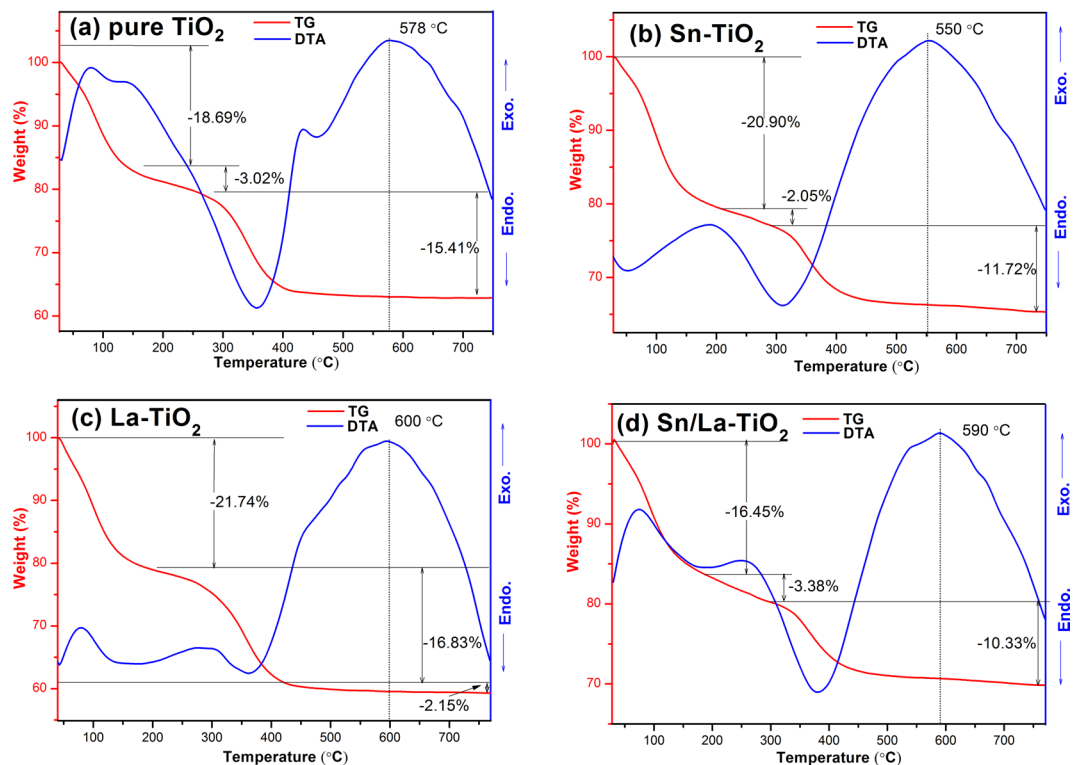
Figure 2. TG and DTA curves for pure TiO$_2$ (**a**), Sn-TiO$_2$ (**b**), La-TiO$_2$ (**c**) and Sn/La-TiO$_2$ (**d**).

indicates that the phase transformation from anatase to rutile begin[5]. For Sn-TiO$_2$ and La-TiO$_2$, the exothermic peaks are approximately at 550 °C and 600 °C, respectively, which make clear that the phase transformation is promoted by Sn doping and is restrained by La doping. This is in accordance with XRD analysis and other literature[25,28]. It's remarkable that the exothermic peak of Sn/La-TiO$_2$ is approximately at 590 °C, suggesting that the phase transformation temperature of Sn/La-TiO$_2$ is higher than that of pure TiO$_2$. That means the La doping plays a leading role in the phase transformation process. This result also agrees well with XRD analysis.

SEM and EDS analyses.   Figure 3 presents the SEM images of pure TiO$_2$ (a) and Sn/La-TiO$_2$ (b) annealed at 450 °C. It is observed that pure TiO$_2$ consists of agglomerated bulks which show different shapes and sizes. The diameter of aggregates in pure TiO$_2$ ranges from 20–1000 nm. Sn/La-TiO$_2$ presents relative uniform particles distribution and the particles show smaller size. The smaller particle size is favorable for the utilization of light source[39].

EDS tests were carried out to examine the element composition of pure and Sn/La-TiO$_2$ annealed at 450 °C and the results are shown in Fig. 3c,d. The peaks of C, Ti, O elements can be observed in the spectrum of pure TiO$_2$. The peak of C derives from conductive plastic which was used in the EDS testing process. Except the peaks of C, Ti, O elements, the peaks of La and Sn elements appear in the spectrum of Sn/La-TiO$_2$, which confirms that La and Sn elements exist in co-doped TiO$_2$ nanomaterials.

TEM analysis.   Figure 4 shows the TEM images of (a) pure TiO$_2$ and (b) Sn/La-TiO$_2$. It can be found that the average size of pure TiO$_2$ is about 15 nm. Sn/La-TiO$_2$ presents smaller size compared to pure TiO$_2$, which is in accordance with the XRD results. In order to precisely investigate the structure of pure TiO$_2$ and Sn/La-TiO$_2$, further studies were carried out with a high-resolution transmission electron microscopy (HRTEM) and the images of pure TiO$_2$ and Sn/La-TiO$_2$ are shown in Fig. 4(c,d), respectively. The lattice fringes are clearly observed, which means that both pure TiO$_2$ and Sn/La-TiO$_2$ nanocrystalline form with good crystallinity[40]. The visible fringe spacings are 0.353 nm in Fig. 4(c) and 0.364 nm in Fig. 4(d), which can be assigned to the (101) plane of anatase TiO$_2$. The (101) plane spacing of Sn/La-TiO$_2$ increases due to the fact that the radius of Sn^{4+} (0.069 nm) is larger than that of Ti^{4+} (0.0605 nm), which indicates that Sn^{4+} ions have entered into TiO$_2$ lattices[27].

XPS analysis.   In order to confirm the chemical states of elements in pure TiO$_2$ and Sn/La-TiO$_2$ annealed at 450 °C, XPS analysis was further carried out and the results are shown in Fig. 5. Figure 5(a) is the total spectra, which demonstrates that both pure TiO$_2$ and Sn/La-TiO$_2$ contain C, Ti, O elements. Besides, the peak of Sn 3d appears in the pattern of Sn/La-TiO$_2$, indicating that Sn exists in TiO$_2$ sample by doping. The absence of La element is probably because the low content of La is below the limit of XPS detection. The C 1 s peaks are mainly attributed to the oil pollution from equipment.

The high-resolution spectra of Ti 2p of pure TiO$_2$ and Sn/La-TiO$_2$ are shown in Fig. 5(b). It can be clearly observed that Ti 2p of pure TiO$_2$ consists of two peaks at 458.40 eV and 464.09 eV, which correspond to Ti 2p$_{3/2}$ and Ti 2p$_{1/2}$, respectively. The slitting between Ti 2p$_{3/2}$ and Ti 2p$_{1/2}$ is 5.69 eV, which is convinced that Ti element
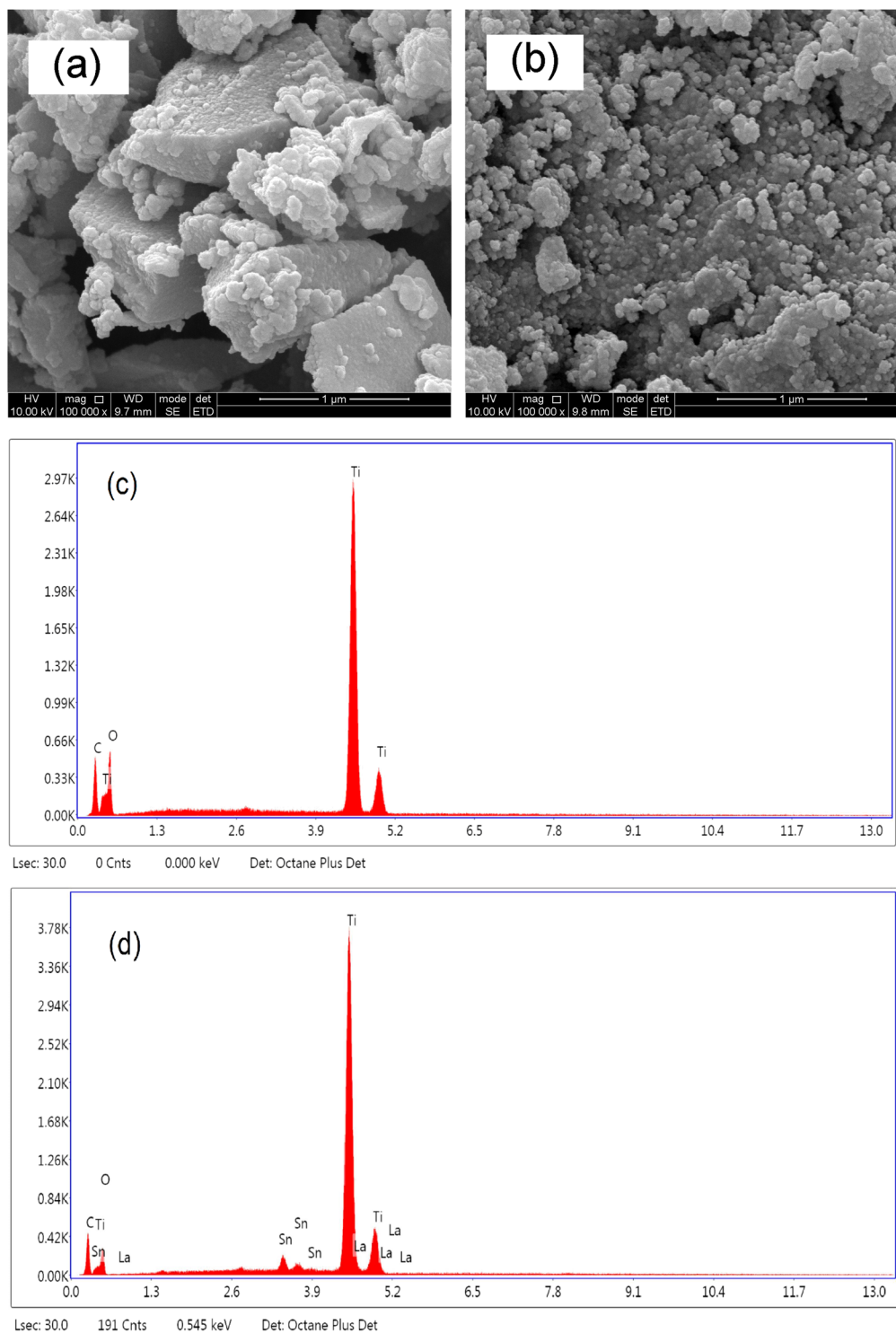
Figure 3. SEM images of pure TiO_2 (**a**) and Sn/La-TiO_2 (**b**) annealed at 450 °C and EDS spectra of pure TiO_2 (**c**) and Sn/La-TiO_2 (**d**) annealed at 450 °C.

exists in the form of Ti^{4+}. Similar to pure TiO_2, Ti 2p of Sn/La-TiO_2 also consists of Ti $2p_{3/2}$ and Ti $2p_{1/2}$ peaks, which are located at 458.49 eV and 464.11 eV, respectively. The slitting of these two peaks is 5.62 eV, that means Ti element is also +4 state in Sn/La-TiO_2[41,42].

Figure 5(c) shows the high-resolution of Sn 3d spectrum. The peaks at 486.08 eV and 494.80 eV ascribe to Sn $3d_{5/2}$ and Sn $3d_{3/2}$, respectively, indicating that Sn element exists as Sn^{4+} [27,28].

The high-resolution spectra of O 1 s of pure TiO_2 and Sn/La-TiO_2 are shown in Fig. 5(d). The peaks of pure TiO_2 at 529.85 eV and 531.83 eV can be attributed to lattice oxygen (O^{2-}) and surface hydroxyl groups (OH^-), respectively[11,35]. Meanwhile, the peaks of lattice oxygen and surface hydroxyl groups for Sn/La-TiO_2 are at
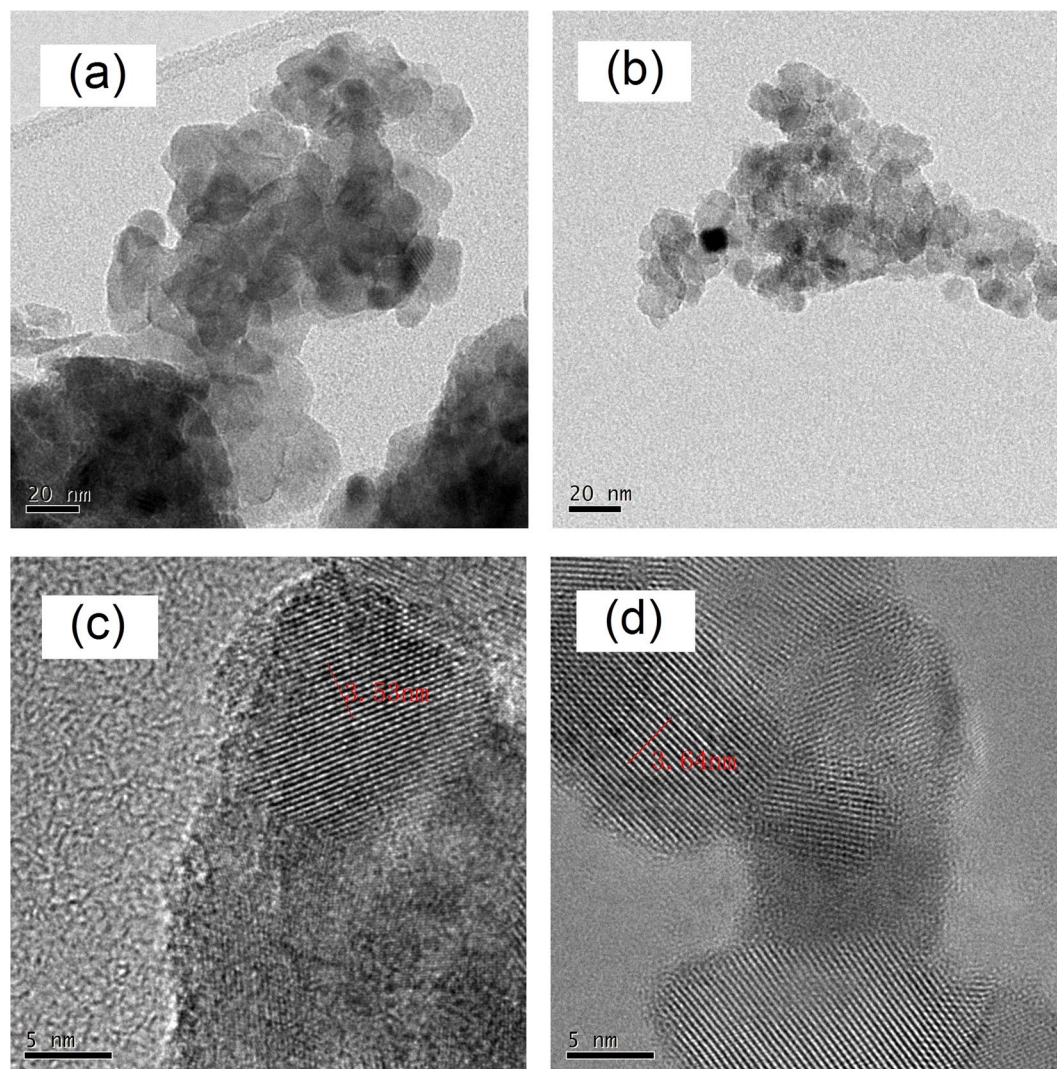
Figure 4. TEM images of pure TiO_2 (**a**) and Sn/La-TiO_2 (**b**) and HRTEM images of pure TiO_2 (**c**) and Sn/La-TiO_2 (**d**) annealed at 450 °C.

530.12 eV and 532.27 eV. It is interesting to note that the proportion of surface hydroxyl groups in Sn/La-TiO_2 is 18.1%, which is higher than that of pure TiO_2 (16.6%). The extra surface hydroxyl groups are profitable to photocatalytic activity because the surface hydroxyl groups can be transformed into hydroxyl radicals, which decompose dye molecules effectively[11].

DRS analysis.   Figure 6 shows the DRS spectra of pure TiO_2, Sn-TiO_2, La-TiO_2 and Sn/La-TiO_2 calcined at 450 °C. The band gap energy (Eg) of samples can be calculated by the equation:

$$(\alpha h\nu)^{1/2} = A\,(h\nu - Eg),$$

where α is the absorption coefficient, $h\nu$ is the photon energy and A is a constant[6]. The band gap energy of pure TiO_2, Sn-TiO_2, La-TiO_2 and Sn/La-TiO_2 are determined to be 3.22 eV, 3.27 eV, 3.35 eV and 3.17 eV, respectively. Sn or La as the doping elements always lead to red shift of TiO_2 as reported before[27,43], however, in this work, Sn-TiO_2 and La-TiO_2 show faint blue shift compared to pure TiO_2. Bhange *et al.*[28] believe that the blue shift is not owing to the quantum size effect since the grain size of TiO_2 is larger than 10 nm, but is the result of the interaction between doping elements and TiO_2 lattice and the formation of new energy levels. Sn/La-TiO_2 shows slight red shift, which proves that the absorption of light improves by Sn and La co-doping.

PL analysis.   It is well known that photoluminescence spectrum results from the recombination of photogenerated electrons and holes[29,31,35]. Therefore, in order to investigate the recombination and separation of photogenerated pairs, photoluminescence measurement was carried out and the results are shown in Fig. 7. The PL spectra of pure TiO_2, Sn-TiO_2, La-TiO_2 and Sn/La-TiO_2 calcined at 450 °C exhibit similar shape, however, the intensities of the samples are different. Pure TiO_2 shows the maximal PL intensity compared to doped TiO_2, suggesting that the recombination of photogenerated electrons and holes is restrained through Sn or La doping. It is noteworthy
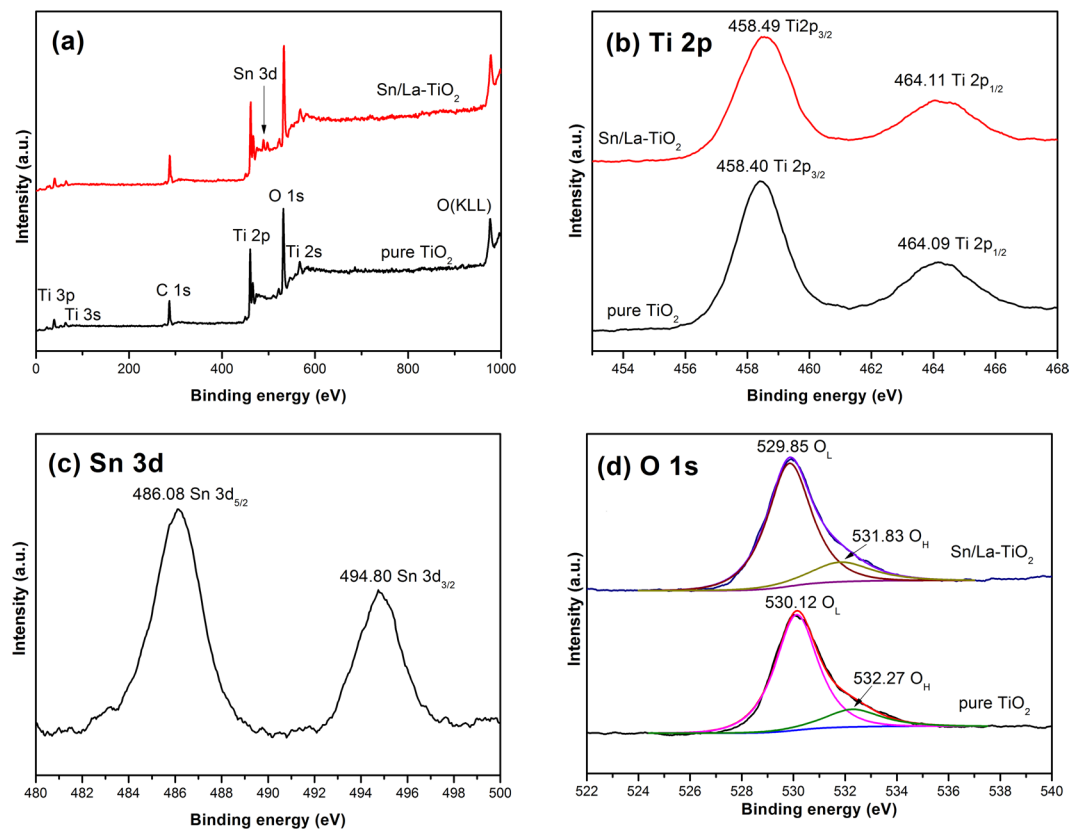
Figure 5. XPS spectra of pure TiO_2 and Sn/La-TiO_2 annealed at 450 °C. Total spectra (**a**), high resolution spectra of Ti 2p (**b**), high resolution spectrum of Sn 3d (**c**) and high resolution spectra of O 1 s (**d**).
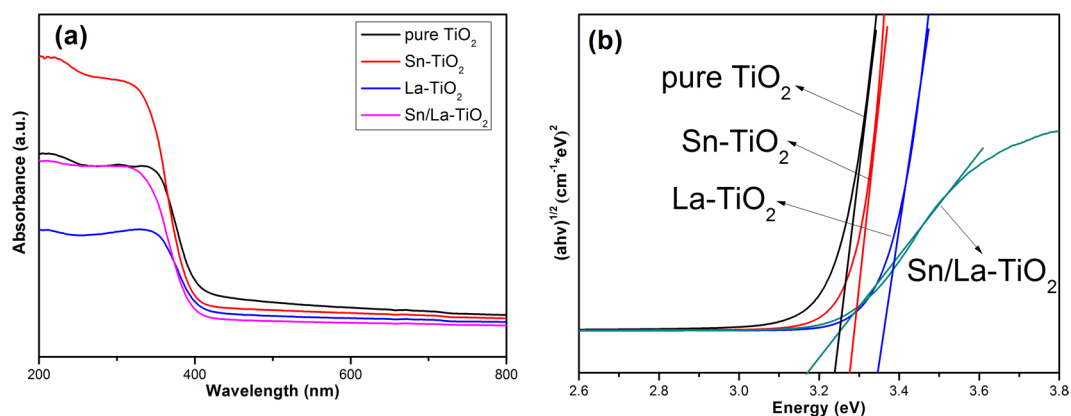

Figure 6. Diffuse reflection spectra of pure TiO_2, Sn-TiO_2, La-TiO_2 and Sn/La-TiO_2 annealed at 450 °C (**a**); plots of $(\alpha h v)^{1/2}$ versus the photon energy (hv) (**b**).

that the PL intensity of Sn/La-TiO_2 is minimal, which indicates that Sn/La-TiO_2 possesses the minimal recombination rate and the maximum separation rate of photogenerated pairs. The higher separation rate is beneficial to photocatalytic activity.

BET analysis. From SEM images results, it is obvious that the aggregation is relieved and the particle size is decreased by Sn and La co-doping. In order to verify that the surface area of TiO_2 is increased after co-doping, nitrogen adsorption-desorption isotherm measurement along with BET measurement is carried out and the N_2 adsorption-desorption isotherms of pure TiO_2 and Sn/La-TiO_2 calcined at 450 °C are shown in Fig. 8. The BET specific surface areas of pure TiO_2 and Sn/La-TiO_2 are determined to be 4.4 $m^2.g^{-1}$ and 85.7 $m^2.g^{-1}$, respectively. The results manifest that Sn/La-TiO_2 exhibits higher surface area than pure TiO_2. The higher surface area is beneficial for the utilization of light source, which is able to improve photocatalytic activity[32].
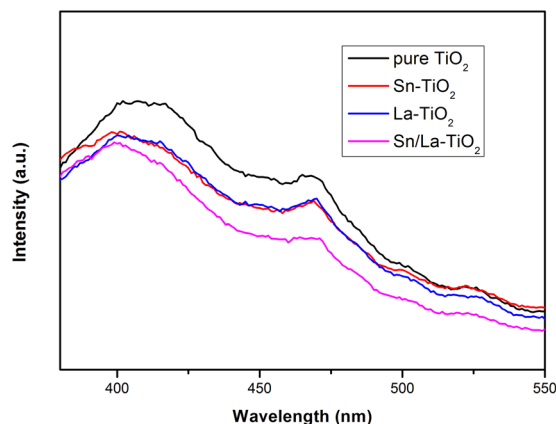
Figure 7. Photoluminescence spectra of pure TiO_2, Sn-TiO_2, La-TiO_2 and Sn/La-TiO_2 annealed at 450 °C.
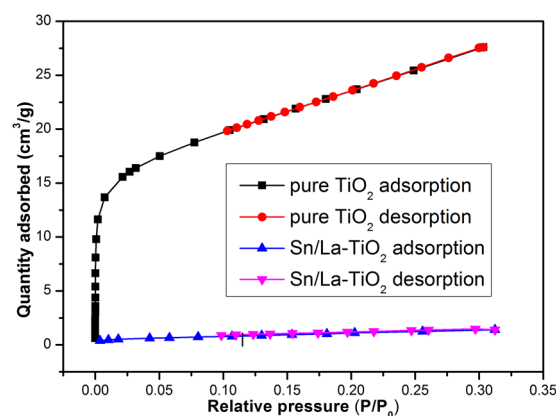

Figure 8. Nitrogen adsorption-desorption isotherm curves of pure TiO_2 and Sn/La-TiO_2 annealed at 450 °C.

Photocatalytic activity. The degradation of RhB was employed to evaluate the photocatalytic activity of the prepared TiO_2 photocatalysts. Figure 9 shows the photocatalytic activity of Sn-TiO_2 and La-TiO_2 with different contents annealed at 450 °C.

The adsorption of RhB molecules was investigated via testing the degradation of RhB with catalyst adding under dark condition. The degradation rate of RhB is 3.2% on the condition of pure TiO_2 adding in darkness, which is ascribed to the adsorption of RhB molecules on the surface of TiO_2[44]. The self degradation of RhB without photocatalyst is 7%, which is negligible in the evaluation. Therefore, the degradation of RhB mainly is derived from the presence of photocatalysts under irradiation.

The degradation rate of pure TiO_2 is 82.5% and all of the doped TiO_2 show higher degradation rates. The optimal doping concentration for La-TiO_2 is 0.5% and for Sn-TiO_2 is 3%. Therefore, the molar ratios of Sn/La-TiO_2 are determined to be La 0.5% and Sn 3%. The degradation rates of pure TiO_2, Sn-TiO_2, La-TiO_2 and Sn/La-TiO_2 annealed at 360 °C, 450 °C and 600 °C are shown in Fig. 10.

The degradation rates of pure TiO_2 annealed at 360 °C, 450 °C and 600 °C are 64.7%, 82.5% and 48.0%, respectively. TiO_2 annealed at 450 °C possesses the best photocatalytic activity than that of 360 °C and 600 °C. As discussed in XRD analysis, pure TiO_2 annealed at 450 °C shows better crystalline integrity of anatase phase compared to 360 °C, which is positive for photocatalytic activity[45]. Meanwhile, pure TiO_2 forms rutile phase at 600 °C and the high rutile content leads to poor photocatalytic activity[46,47]. Significantly, all of the doped TiO_2 photocatalysts exhibit higher photocatalytic performance than pure TiO_2 at three temperatures. The degradation rates of RhB for Sn/La-TiO_2 are 98.1%, 99.1% and 97.9% at the annealing temperatures of 360 °C, 450 °C and 600 °C, which are 1.52 times, 1.20 times, 2.04 times higher than that of pure TiO_2.

From XRD analysis, it can be noted that there is no peak for Sn, La and their oxides. Since the radius of La^{3+} (0.1061 nm) is much bigger than that of Ti^{4+} ion (0.0605 nm). Therefore, it is hard for La^{3+} ions to substitute Ti^{4+} ions in TiO_2 lattice and it is reasonable to suppose that La^{3+} ions is located at the surface of TiO_2[23,24,48]. La^{3+} ions act charge carrier trapping centers on the surface of TiO_2, which suppresses the recombination of photogenerated electron-hole pairs and prolongs the lifetime, thus boosts the photocatalytic activity[23,49]. On the other hand, as the radius of Sn^{4+} ion is close to Ti^{4+} ion, Sn^{4+} ions are likely to substitute Ti^{4+} ions in the lattice of TiO_2 and causes lattice distortion, which creates more surface defects. The surface defects are beneficial for the formation of oxygen vacancies and generating more superoxide radicals which degrade RhB molecules effectively[20,27,28]. Compared to pure and single element doped TiO_2, Sn/La-TiO_2 shows the highest photocatalytic activities at three
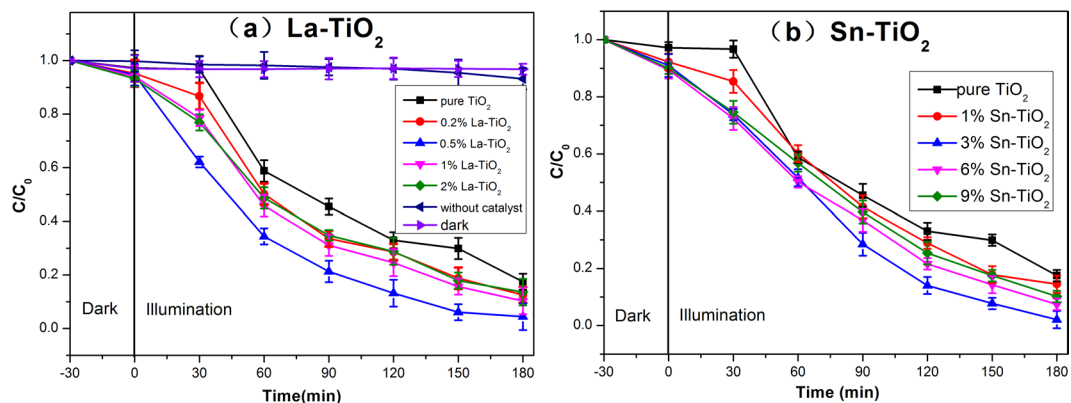
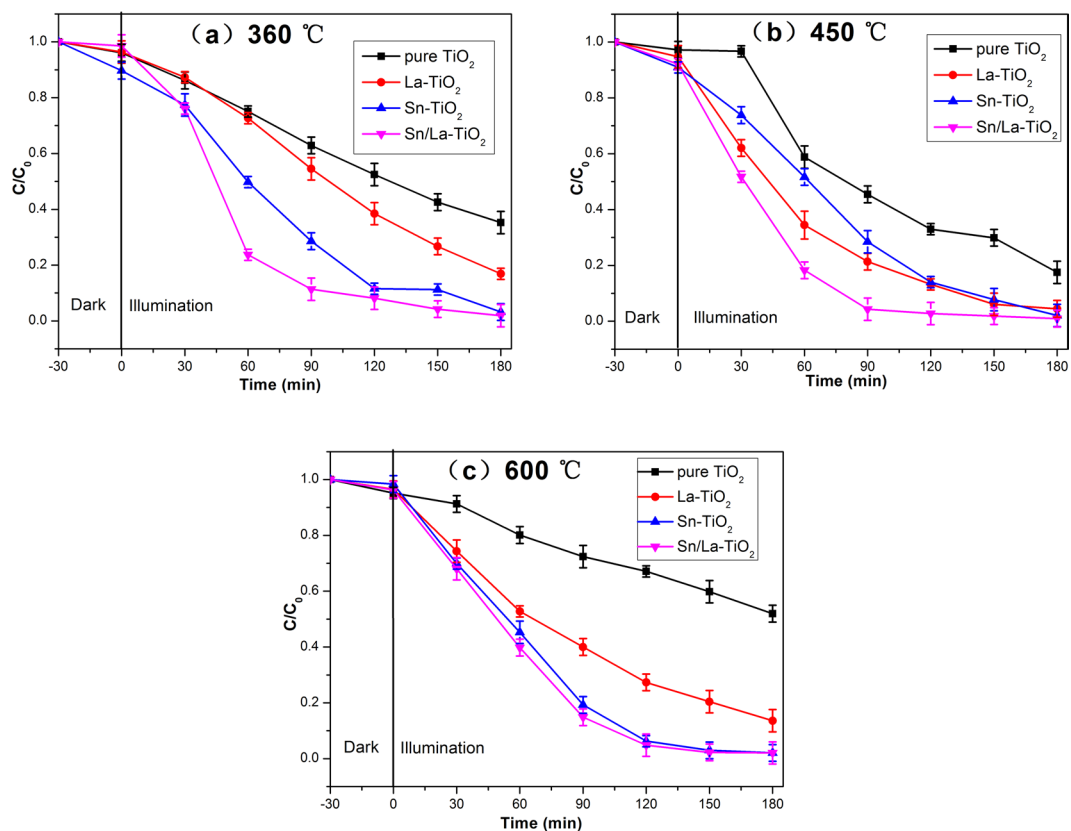**Figure 9.** Photocatalytic degradation of RhB using (**a**) La-TiO$_2$ and (**b**) Sn-TiO$_2$.

Figure 10. Photocatalytic degradation of RhB for pure TiO$_2$, Sn-TiO$_2$, La-TiO$_2$ and Sn/La-TiO$_2$ annealed at 360 °C (**a**), 450 °C (**b**) and 600 °C (**c**).

temperatures because both Sn and La could enhance the photocatalytic activity as discussed before and Sn-La co-doping produces a synergistic effect. Moreover, from the results of XPS analysis, it is clear that the surface hydroxyl groups increase via Sn, La co-doping, which is propitious to promote photocatalytic activity. Besides, more surface area caused by Sn, La co-doping is also in favor of the enhancement of photocatalytic activity[23,27].

Figure 11 presents the kinetic fitting plots of ln (C/C$_0$) against irradiation time t for the photocatalysts, which show linear relationships, indicating that the degradation of RhB by TiO$_2$ photocatalysts follows pseudo first order kinetics[41]. The apparent reaction rate constant k is calculated by:

$$\ln(C/C_0) = -k\,t$$

where t is the reaction time, C and C$_0$ are the concentration at time t and the initial concentration of RhB solution, respectively.
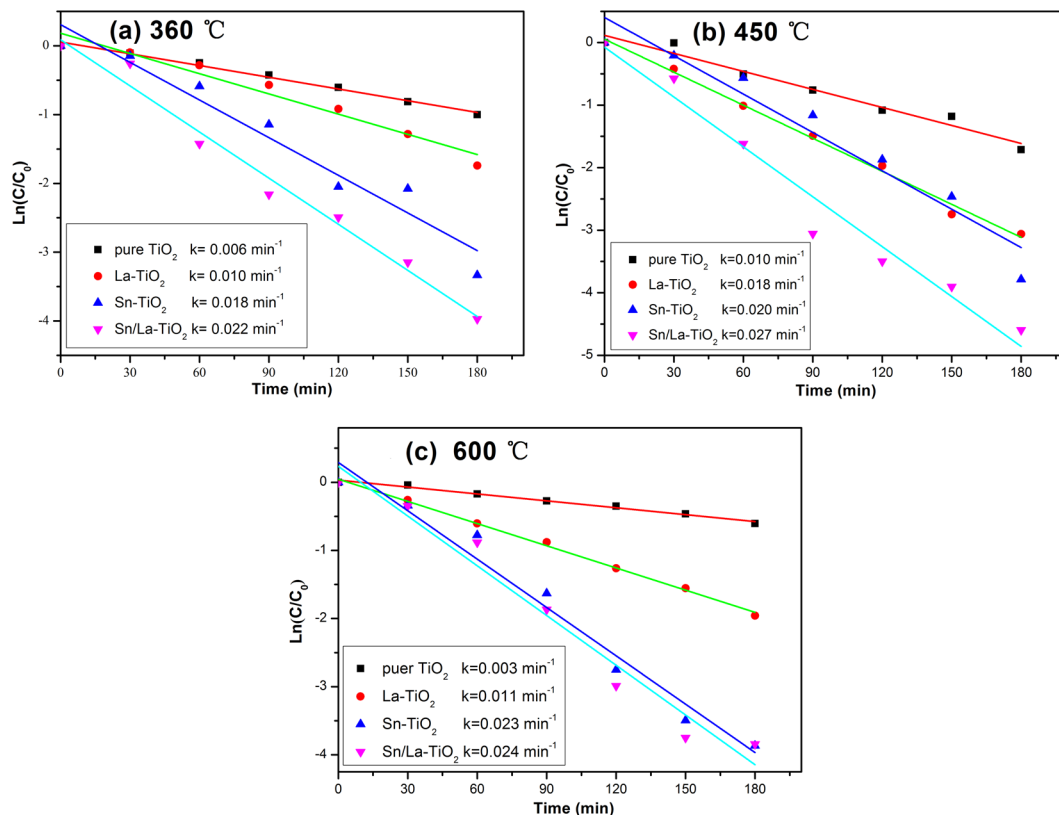
Figure 11. First-order reaction rate constants k against reaction time for different photocatalysts annealed at 360 °C (**a**), 450 °C (**b**) and 600 °C (**c**).
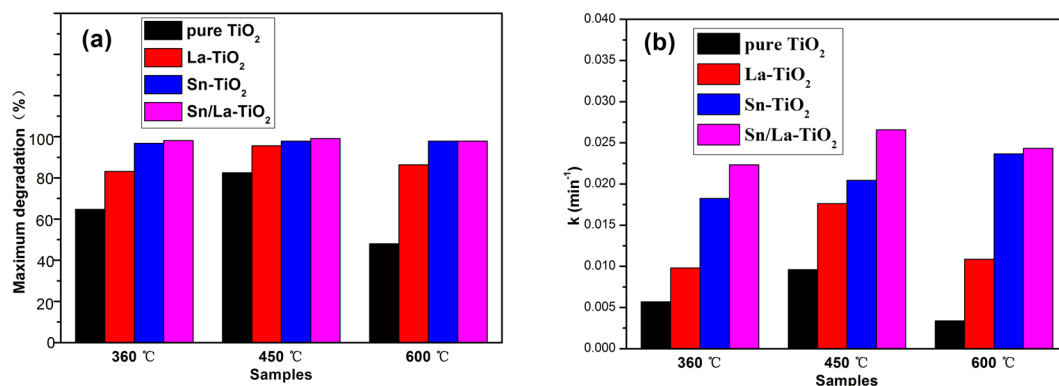

Figure 12. Comparison charts of degradation rates (**a**) and reaction rate constants k (**b**) for all of the photocatalysts.

The ultimate degradation rates after 180 min and the apparent reaction rate constant k of all the photocatalysts are shown in Fig. 12 for a better comparison. The Sn/La-TiO$_2$ also exhibit the fastest reaction rate and the apparent reaction rate constant k are 0.022 min^{-1}, 0.027 min^{-1} and 0.024 min^{-1} at 360 °C, 450 °C and 600 °C, which are 3.7 times, 2.7 times and 8 times more than that of pure TiO$_2$. The photocatalytic performance of TiO$_2$ can be enhanced remarkably by Sn and La co-doping and the most noticeable enhancement effect occurs at the heat treatment temperature of 600 °C. The degradation data for all of the catalysts are shown in Table 2.

In order to study the effect of catalyst dosage, temperature, pH value and recyclability on the photocatalytic activity of catalyst, pure TiO$_2$ annealed at 450 °C was chosen for the experiments.

In Fig. 13(a), the comparison of the degradation rate obtained with 0.25 g/L, 0. 5 g/L, 1 g/L, 1.5 g/L and 2 g/L catalyst is shown. The degradation rate increases with raising catalyst amount and the enhancement of degradation rate can be attributed to more surface area[50]. However, the degradation rate increases slightly when the concentration of catalyst surpasses 1 g/L. The aggregation of TiO$_2$ particles occurs when the catalyst dosage is at high level, which leads to a decrease in surface area[51].

Temperature	Samples	Degradation rate	k (min^{-1})	R^2
360 °C	pure TiO$_2$	64.7%	0.006	0.989
	Sn-TiO$_2$	96.8%	0.018	0.938
	La-TiO$_2$	83.1%	0.010	0.954
	Sn/La-TiO$_2$	98.1%	0.022	0.980
450 °C	pure TiO$_2$	82.5%	0.010	0.962
	Sn-TiO$_2$	97.9%	0.020	0.932
	La-TiO$_2$	95.6%	0.018	0.993
	Sn/La-TiO$_2$	99.1%	0.027	0.961
600 °C	pure TiO$_2$	48.0%	0.003	0.986
	Sn-TiO$_2$	97.9%	0.023	0.970
	La-TiO$_2$	86.4%	0.011	0.997
	Sn/La-TiO$_2$	97.9%	0.024	0.961

Table 2. Degradation rates of RhB (a) and reaction rate constants k (b) of photocatalysts.
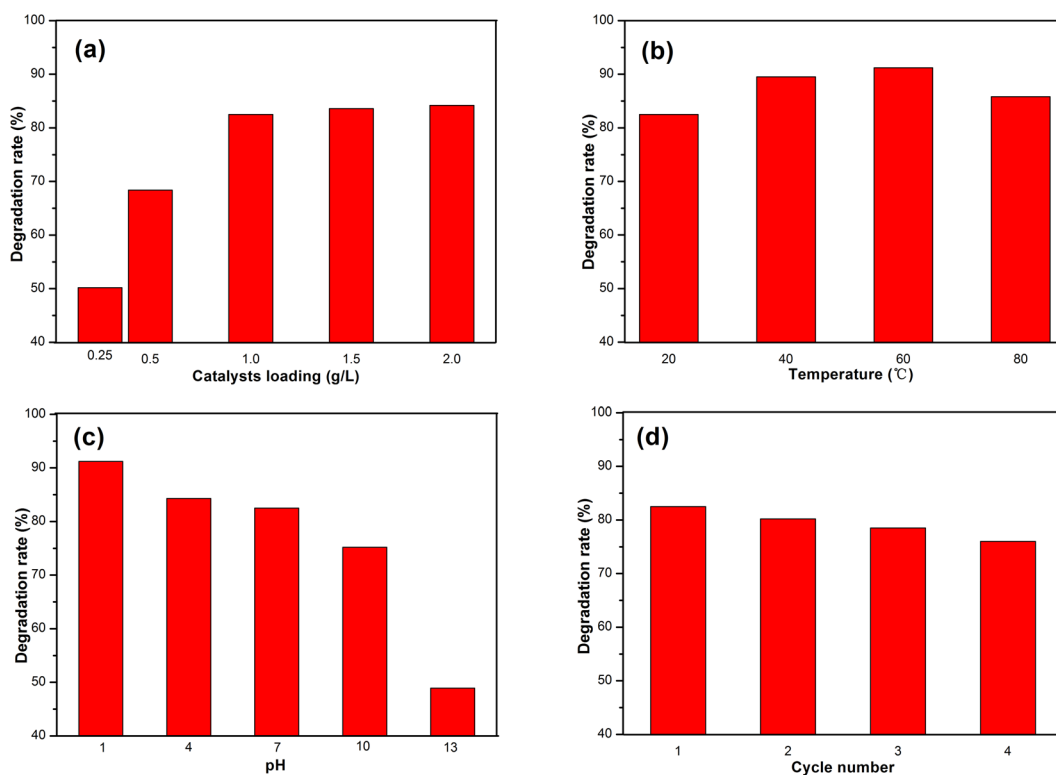

Figure 13. The effect of catalyst dosage, temperature, pH value and recyclability on the photocatalytic activity of catalyst.

The effect of temperature on the degradation rate of catalyst was studied by performed the photocatalytic experiments under temperatures ranging from 20 °C to 80 °C and the results are shown in Fig. 13(b). The degradation rare first increases when the temperature reach 60 °C and then decreases when the temperature is up to 80 °C. The oxidation rate of RhB molecules enhances with increase in temperature[50]. However, more rising the temperature is harmful to the photocatalytic activity because the recombination rate of photogenerated pairs and the desorption process of RhB molecules increase[51].

In order to study the impact of the pH value on the degradation of RhB by catalyst, RhB solution was adjusted to different pH value (1, 4, 7, 10 and 13) by HCl (1 mol/L) and NaOH (1 mol/L). The results in Fig. 13(c) show that the degradation rate can be changed by varying the pH value. Acid environment shows higher degradation rate than neutral and alkaline environment. The PZC of pure TiO$_2$ is about 6.25, therefore, the adsorption on catalyst is poor in alkaline solution. Acid solution is beneficial for reducing agglomeration and the formation of hydroxyl radicals, which lead to higher photocatalytic activity[50].

The photocatalytic experiment was repeated four cycles to test the reusability of pure TiO$_2$ catalyst and the results are shown in Fig. 13(d). The degradation rate after four cycles is 76.0%, which is slightly lower than that of the first cycle (82.5%). The decrease in the degradation rate can be attributed to the loss in adsorption between TiO$_2$ catalyst and RhB molecules[44].
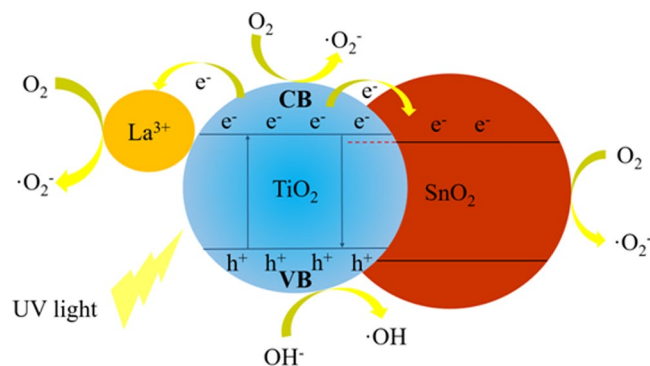
Figure 14. The schematic diagram of band structure and electron pairs separation in Sn/La-TiO₂.

The schematic diagram of band structure and electron pairs separation in Sn/La-TiO$_2$ is shown in Fig. 14. The electrons in valence band (VB) are excited to conduction band (CB) when TiO$_2$ catalyst is irradiated by UV light, leaving holes in valence band[52]. On the one hand, La^{3+} ions which on the surface of TiO$_2$ can trap the photogenerated electrons in conduction band, consequently, the recombination of electrons and pairs is retarded and the photogenerated pairs are separated effectively[47]. On the other hand, the photogenerated electrons in conduction band of TiO$_2$ can be transferred to conduction band of SnO$_2$, since the conduction band energy level of SnO$_2$ is lower than that of TiO$_2$[19,53,54]. Both Sn and La species are beneficial for the separation of photogenerated pairs, therefore, more electrons and holes can be involved into the photocatalytic degradation of RbB molecules. The holes combine with hydroxyl ions (OH$^-$) to form hydroxyl radicals (.OH) and the electrons combine with adsorbed oxygen (O$_2$) to form super-oxygen ions (.O$_2^-$)[3,54]. The resulting radicals degrade RbB molecules into smaller hydrocarbons and finally to CO$_2$ and H$_2$O[55].

Conclusions

In summary, pure TiO$_2$, Sn-TiO$_2$, La-TiO$_2$ and Sn/La-TiO$_2$ nanomaterials experienced different temperature heat treatment were successfully synthesized via sol-gel route. The photocatalytic activity of the prepared TiO$_2$ photocatalysts under UV light were tested by the degradation of RhB. Calcination temperature has an obvious influence on the photocatalytic property of pure TiO$_2$ and it shows the best degradation rate at 450 °C. Doping with Sn and La enhances the photocatalytic activity of TiO$_2$ significantly at three temperatures and Sn/La-TiO$_2$ exhibit the highest degradation rates. The effect of co-doping on the improvement of photocatalytic performance can be attributed to the synergistic effect in suppressing photogenerated pairs and the formation of extra surface hydroxyl groups and more surface area involved during the reaction process.

References

1. Mishra, Y. K. & Adelung, R. ZnO tetrapod materials for functional applications. *Materials Today*. https://doi.org/10.1016/j.mattod.2017.11.003.
2. Jin, Y. *et al*. Hollow Zn$_x$ Cd$_{1-x}$ S nanospheres with enhanced photocatalytic activity under visible light. *Scientific Reports*. **6**, 2997–3004 (2016).
3. Tripathi, K. M., Tran, T. S., Kim, Y. J. & Kim, T. Y. Green fluorescent onion-like carbon nanoparticles from flaxseed oil for visible light induced photocatalytic applications and label-free detection of Al(III) ions. *ACS Sustainable Chemistry & Engineering*. **5**, 3982–3992 (2017).
4. Mena, E., Rey, A., Rodríguez, E. M. & Beltrán, F. J. Reaction mechanism and kinetics of DEET visible light assisted photocatalytic ozonation with WO$_3$ catalyst. *Applied Catalysis B: Environmental*. **202**, 460–472 (2017).
5. Sahnesarayi, M. K., Sarpoolaky, H. & Rastegari, S. Effect of heat treatment temperature on the performance of nano-TiO$_2$ coating in protecting 316L stainless steel against corrosion under UV illumination and dark conditions. *Surface & Coatings Technology*. **258**, 861–870 (2014).
6. Shaban, M., Ashraf, A. M. & Abukhadra, M. R. TiO$_2$ Nanoribbons/carbon nanotubes composite with enhanced photocatalytic activity; fabrication, characterization, and application. *Scientific Reports*. **8**, 781–798 (2018).
7. Li, L. H. *et al*. The effects of Cu-doped TiO$_2$ thin films on hyperplasia, inflammation and bacteria infection. *Applied Sciences*. **5**, 1016–032 (2015).
8. Shang, J., Xu, W. W., Ye, C. X., George, C. & Zhu, T. Synergistic effect of nitrate-doped TiO$_2$ aerosols on the fast photochemical oxidation of formaldehyde. *Scientific Reports*. **7**, 1–9 (2017).
9. Iwasaki, M., Hara, M., Kawada, H., Tada, H. & Ito, S. Cobalt ion-doped TiO$_2$ photocatalyst response to visible light. *Journal of Colloid and Interface Science*. **224**, 202–204 (2000).
10. Lin, H. J., Yang, T. S., Hsi, C. S., Wang, M. C. & Lee, K. C. Optical and photocatalytic properties of Fe^{3+}-doped TiO$_2$ thin films prepared by a sol-gel spin coating. *Ceramics International*. **40**, 10633–10640 (2014).
11. Demirci, S. *et al*. Synthesis and characterization of Ag doped TiO$_2$ heterojunction films and their photocatalytic performances. *Applied Surface Science*. **390**, 591–601 (2016).
12. Deng, X. Q., Liu, J. L., Li, X. S., Zhu, B. & Zhu, X. B. Kinetic study on visible-light photocatalytic removal of formaldehyde from air over plasmonic Au/TiO$_2$. *Catalysis Today*. **281**, 630–635 (2017).
13. Yang, Z. L., Lu, J., Ye, W. C., Yu, C. S. & Chang, Y. L. Preparation of Pt/TiO$_2$ hollow nanofibers with highly visible light photocatalytic activity. *Applied Surface Science*. **392**, 472–480 (2017).
14. Liu, Y., Xie, C. S., Li, J., Zou, T. & Zeng, D. New insights into the relationship between photocatalytic activity and photocurrent of TiO$_2$/WO$_3$ nanocomposite. *Applied Catalysis A: General*. **433–434**, 81–87 (2012).
15. El-Lateef, H. M. A. & Khalaf, M. M. Corrosion resistance of ZrO$_2$-TiO$_2$ nanocomposite multilayer thin films coated on carbon steel in hydrochloric acid solution. *Materials Characterization*. **108**, 29–41 (2015).

16. Li, J., Lin, C. J., Li, J. T. & Lin, Z. Q. A photoelectrochemical study of CdS modified TiO₂ nanotube arrays as photoanodes for cathodic protection of stainless steel. *Thin Solid Films.* **519**, 5494–5502 (2011).

17. Zhu, Y. F. *et al.* Fabrication of heterostructured SrTiO₃/TiO₂ nanotube array films and their use in photocathodic protection of stainless steel. *Electrochimica Acta.* **121**, 361–368 (2014).

18. Mazur, M., Morgiel, J., Wojcieszak, D., Kaczmarek, D. & Kalisz, M. Effect of Nd doping on structure and improvement of the properties of TiO₂ thin films. *Surface & Coatings Technology.* **270**, 57–65 (2015).

19. Du, J. M. *et al.* Synthesis and enhanced photocatalytic activity of black porous Zr-doped TiO₂ monoliths. *Nano.* **11**, 1650068–1650075 (2016).

20. Mohamed, R. M. & Aazam, E. S. Effect of Sn loading on the photocatalytic aniline synthesis activity of TiO₂ nanospheres. *Journal of Alloys and Compounds.* **595**, 8–13 (2014).

21. Wang, W., Liu, Y., Qu, J. F., Chen, Y. B. & Shao, Z. P. Nitrogen-doped TiO₂ microspheres with hierarchical micro/nanostructures and rich dualphase junctions for enhanced photocatalytic Activity. *RSC Advances.* **6**, 40923–40931 (2016).

22. Bakar, S. A. & Ribeiro, C. Rapid and morphology controlled synthesis of anionic S-doped TiO₂ photocatalysts for visible-light-driven photodegradation of organic pollutants. *RSC Advances.* **6**, 36516–36527 (2016).

23. Nešić, J. *et al.* Preparation, characterization and photocatalytic activity of lanthanum and vanadium co-doped mesoporous TiO₂ for azo-dye degradation. *Journal of Molecular Catalysis A: Chemical.* **378**, 67–75 (2013).

24. Peng, H., Cui, J., Zhan, H. J. & Zhang, X. Improved photodegradation and detoxification of 2,4,6-trichlorophenol by lanthanum doped magnetic TiO₂. *Chemical Engineering Journal.* **264**, 316–321 (2015).

25. Xin, Y. J. & Liu, H. L. Study on mechanism of photocatalytic performance of La-doped TiO₂/Ti photoelectrodes by theoretical and experimental methods. *Journal of Solid State Chemistry.* **184**, 3240–3246 (2011).

26. Solís-Casados, D. A., Escobar-Alarcón, L., Gómez-Ol iván, L. M., Haro-Poniatowski, E. & Klimova, T. Photodegradation of pharmaceutical drugs using Sn-modified TiO₂ powders under visible light irradiation. *Fuel.* **198**, 3–10 (2017).

27. Li, J. L. *et al.* Sn doped TiO₂ nanotube with oxygen vacancy for highly efficient visible light photocatalysis. *Journal of Alloys and Compounds.* **679**, 454–462 (2016).

28. Bhange, P. D., Awate, S. V., Gholap, R. S., Gokavi, G. S. & Bhange, D. S. Photocatalytic degradation of methylene blue on Sn-doped titania nanoparticles synthesized by solution combustion route. *Materials Research Bulletin.* **76**, 264–272 (2016).

29. Zhang, P. F., Li, X. W., Wu, X. K., Zhao, T. X. & Wen, L. S. Influence of In³⁺-doping and Ag⁰-depositing on the visible-light-induced photocatalytic activity of TiO₂. *Journal of Alloys and Compounds.* **673**, 405–410 (2016).

30. Zhang, W. *et al.* Preparation, characterization, and photocatalytic activity of boron and lanthanum co-doped TiO₂. *Catalysis Communications.* **45**, 144–147 (2014).

31. Tripathi, A. K. *et al.* Structural, optical and photoconductivity of Sn and Mn doped TiO₂ Nanoparticles. *Journal of Alloys and Compounds.* **622**, 37–47 (2015).

32. Zhang, H. *et al.* Ni²⁺ and Ti³⁺ co-doped porous black anatase TiO₂ with unprecedented-high visible-light-driven photocatalytic degradation performance. *RSC Advances.* **5**, 107150–107157 (2015).

33. Naraginti, S. *et al.* Enhanced photo-catalytic activity of Sr and Ag co-doped TiO₂ nanoparticles for the degradation of Direct Green-6 and Reactive Blue-160 under UV & visible light. *Spectrochimica Acta Part A: Molecular and Biomolecular Spectroscopy.* **149**, 571–579 (2015).

34. Huang, T. Z. *et al.* Effects of N and F doping on structure and photocatalytic properties of anatase TiO₂ nanoparticles. *RSC Advances.* **37**, 16657–16664 (2013).

35. Lei, X. F., Xue, X. X. & Yang, H. Preparation and characterization of Ag-doped TiO₂ nanomaterials and their photocatalytic reduction of Cr(VI) under visible light. *Applied Surface Science.* **321**, 396–403 (2014).

36. Ding, X. Z., Liu, L., Ma, X. M., Qi, Z. Z. & He, Y. Z. The influence of alumina dopant on the structural transformation of gel-derived nanometre titania powders. *Journal of Materials Science Letters.* **13**, 462–464 (1994).

37. Spurr, R. A. & Myers, H. Quantitative analysis of anatase-rutile mixtures with an X-Ray diffractometer. *Analytical Chemistry.* **29**, 760–762 (1957).

38. Uvarov, V. & Popov, I. Metrological characterization of X-ray diffraction methods for determination of crystallite size in nano-scale materials. *Materials Characterization.* **58**, 883–891 (2007).

39. Dou, L. *et al.* P123-assisted hydrothermal synthesis of BiOI with enhanced photocatalytic performance. *Materials Letters.* **153**, 179–181 (2016).

40. Begum, A., Tripathi, K. M. & Sarkar, S. Water-induced formation, characterization, and photoluminescence of carbon nanotube-based composites of Gadolinium(III) and Platinum(II) dithiolenes. *Chemistry-A European Journal.* **20**, 1–6 (2014).

41. Zhang, Y., Wang, T., Zhou, M., Wang, Y. & Zhang, Z. M. Hydrothermal preparation of Ag-TiO₂ nanostructures with exposed {001}/{101} facets for enhancing visible light photocatalytic activity. *Ceramics International.* **43**, 3118–3126 (2017).

42. Huang, D. G. *et al.* Synthesis of samarium- and nitrogen-co-doped TiO₂ by modified hydrothermal method and its photocatalytic performance for the degradation of 4-chlorophenol. *Journal of Physics and Chemistry of Solids.* **70**, 853–859 (2009).

43. Yu, Y. M. *et al.* A facile one-pot synthesis of N-La codoped TiO₂ porous materials with bio-hierarchical architectures and enhanced photocatalytic activity. *Materials Chemistry and Physics.* **182**, 77–85 (2016).

44. Vaiano, V., Sacco, O., Sannino, D. & Ciambelli, P. Nanostructured N-doped TiO₂ coated on glass spheres for the photocatalytic removal of organic dyes under UV or visible light irradiation. *Applied Catalysis B: Environmental.* **170–171**, 153–161 (2015).

45. Tang, X. K., Feng, Q. M., Lin, K. & Tan, Y. Synthesis and characterization of a novel nanofibrous TiO₂/SiO₂ composite with enhanced photocatalytic activity. *Materials Letters.* **183**, 175–178 (2016).

46. Alves, A. K., Berutti, F. A. & Bergmann, C. P. Visible and UV photocatalytic characterization of Sn-TiO₂ electrospun fibers. *Catalysis Today.* **208**, 7–10 (2013).

47. Ilkhechi, N. N., Akbarpour, M. R., Yavari, R. & Azar, Z. Sn⁴⁺ and La³⁺ co doped TiO₂ nanoparticles and their optical, photocatalytic and antibacterial properties under visible light. *Journal of Materials Science Materials in Electronics.* **28**, 16658–16664 (2017).

48. Bokare, A., Pai, M. & Athawale, A. A. Surface modified Nd doped TiO₂ nanoparticles as photocatalysts in UV and solar light irradiation. *Solar Energy.* **91**, 111–119 (2013).

49. Du, J. M. *et al.* A facile sol-gel method for synthesis of porous Nd-doped TiO₂ monolith with enhanced photocatalytic activity under UV-Vis irradiation. *Microporous and Mesoporous Materials.* **182**, 87–94 (2013).

50. Pazoki, M., Parsa, M. & Farhadpour, R. Removal of the hormones dexamethasone (DXM) by Ag doped on TiO₂ photocatalysis. *Journal of Environmental Chemical Engineering.* **4**, 4426–4434 (2016).

51. Malik, R. *et al.* Nano gold supported on ordered mesoporous WO₃/SBA-15 hybrid nanocomposite for oxidative decolorization of azo dye. *Microporous and Mesoporous Materials.* **225**, 245–254 (2016).

52. Wang, T. Preparation of electrospun Ag/TiO₂ nanotubes with enhanced photocatalytic activity based on water/oil phase separation. *Physica E.* **86**, 103–110 (2017).

53. Tomer, V. K. & Duhan, S. Ordered mesoporous Ag-doped TiO₂/SnO₂ nanocomposite based highly sensitive and selective VOC sensors. *Journal of Materials Chemistry A.* **4**, 1033–1043 (2016).

54. Kadam, A., Dhabbe, R., Shin, D. S., Garadkar, K. & Park, J. Sunlight driven high photocatalytic activity of Sn doped N-TiO₂ nanoparticles synthesized by a microwave assisted method. *Ceramics International.* **43**, 5164–5172 (2017).

55. Khare, P. *et al.* Sunlight-induced selective photocatalytic degradation of methylene blue in bacterial culture by pollutant soot derived nontoxic graphene nanosheets. *ACS Sustainable Chemistry & Engineering.* **6**, 579–589 (2018).

Acknowledgements

Author Contributions

X.D. Zhu and W. Feng designed the experiments, characterized the samples, analyzed the data, and wrote the manuscript. L.X. Pei and R.R. Zhu carried out the specific experimental process and analyzed the data. Y. Jiao carried out TEM tests and photocatalytic tests according to the suggestions of reviewers. R.Y. Tang contributed to the writing of the manuscript.

Additional Information

Competing Interests: The authors declare no competing interests.

Publisher's note: Springer Nature remains neutral with regard to jurisdictional claims in published maps and institutional affiliations.